JCTC Journal of Chemical Theory and Computation

Article

Cite This: J. Chem. Theory Comput. 2018, 14, 3955−3966

pubs.acs.org/JCTC

Photoexcited Nonadiabatic Dynamics of Solvated Push−Pull π-Conjugated Oligomers with the NEXMD Software

Andrew E. Sifain,[†,‡,§] Josiah A. Bjorgaard,[‡,§,∥] Tammie R. Nelson,[‡] Benjamin T. Nebgen,[‡] Alexander J. White,[‡] Brendan J. Gifford,[‡,§,⊥] David W. Gao,[‡,#] Oleg V. Prezhdo,[†,▽] Sebastian Fernandez-Alberti,[○] Adrian E. Roitberg,[◆] and Sergei Tretiak*[,‡,§,¶]

[†]Department of Physics and Astronomy and [▽]Department of Chemistry, University of Southern California, Los Angeles, California 90089, United States

[‡]Theoretical Division, [§]Center for Nonlinear Studies, [∥]Computational Physics Division, and [¶]Center for Integrated Nanotechnologies, Los Alamos National Laboratory, Los Alamos, New Mexico 87545, United States

[⊥]Department of Chemistry and Biochemistry, North Dakota State University, Fargo, North Dakota 58108, United States

[#]Los Alamos High School, Los Alamos, New Mexico 87544, United States

[○]Universidad Nacional de Quilmes/CONICET, Roque Saenz Peña 352, B1876BXD Bernal, Argentina

[◆]Department of Chemistry, University of Florida, Gainesville, Florida 32611, United States

Supporting Information

ABSTRACT: Solvation can be modeled implicitly by embedding the solute in a dielectric cavity. This approach models the induced surface charge density at the solute−solvent boundary, giving rise to extra Coulombic interactions. Herein, the Nonadiabatic EXcited-state Molecular Dynamics (NEXMD) software was used to model the photoexcited nonradiative relaxation dynamics in a set of substituted donor−acceptor oligo(*p*-phenylenevinylene) (PPVO) derivatives in the presence of implicit solvent. Several properties of interest including optical spectra, excited state lifetimes, exciton localization, excited state dipole moments, and structural relaxation are calculated to elucidate dependence of functionalization and solvent polarity on photoinduced nonadiabatic dynamics. Results show that solvation generally affects all these properties, where the magnitude of these effects vary from one system to another depending on donor−acceptor substituents and molecular polarizability. We conclude that implicit solvation can be directly incorporated into nonadiabatic simulations within the NEXMD framework with little computational overhead and that it qualitatively reproduces solvent-dependent effects observed in solution-based spectroscopic experiments.

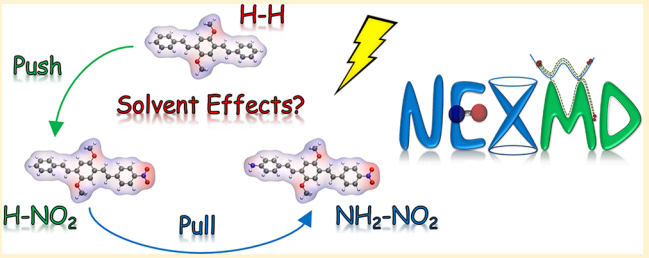

1. INTRODUCTION

Modeling nonadiabatic excited state molecular dynamics is at the core of understanding photoinduced processes such as charge and energy transfer,[1−6] photoisomerization,[7,8] photodissociation,[9,10] and other types of coupled electron−vibrational (or vibronic) dynamics.[11−13] In organic conjugated molecules, photoinduced relaxation occurs in a dense manifold of vibrational and electronic states due to strong electronic correlations and electron−phonon couplings.[14−16] A theoretical understanding of excited state relaxation in these materials not only aids in the design of functional photoactive materials for technological applications,[17−24] but also elucidates photochemical and photophysical properties that frequently go undetected in experiments such as conformational changes, multiple reaction pathways, and electron density distributions.[25,26] Our ability to gain understanding at the molecular level is largely dictated by the reliability of computational methods. Due to the large number of degrees of freedom in a solvent, nonadiabatic simulations of realistically large molecular systems (tens to hundreds of atoms in size) are typically performed in the gas phase, whereas most experiments are carried out by probing solution-based or solid-state samples. The use of qualitatively accurate and numerically efficient methods of modeling solvation are necessary for predicting and interpreting structural, optical, and dynamical properties. Herein, we implement a solvent model in the Nonadiabatic EXcited-state Molecular Dynamics (NEXMD) software and demonstrate its effects on the photoinduced nonadiabatic dynamics in a set of organic conjugated push−pull (or donor−acceptor) molecules.

The solute−solvent system is most accurately modeled by quantum mechanics. However, this approach is prohibitively expensive for systems with multiple degrees of freedom.

Received: January 31, 2018
Published: June 6, 2018

DOI: 10.1021/acs.jctc.8b00103
J. Chem. Theory Comput. 2018, 14, 3955−3966

Therefore, approximations capable of reproducing the effective solvent response in large systems are needed. One such method resorts the portion of solvent interacting with the solute to a quantum mechanical description using a combined quantum mechanical/molecular mechanical (QM/MM) approach.[27−29] At this level, the ab initio molecular dynamics would still require averaging over many solvent configurations.[30−32] Implicit solvent models reduce computational cost even further by treating the solvent as a dielectric continuum—an effective average over many solvent configurations.[33−37] By embedding the solute in a dielectric cavity,[38] charge density of the solute induces a surface charge density in the cavity, producing a polarization that screens Coulombic interactions. Analytical gradients in time-dependent density functional theory (TD-DFT) and time-dependent Hartree−Fock (TD-HF) make it feasible to include solvent effects at the first-order or linear response level.[39−41] In this way, the solvent responds linearly to the excitation of the solute which is determined by the spatial distribution of the transition density.[40,41]

The NEXMD software uses semiempirical Hamiltonians within TD-HF theory, thereby making it feasible to implement a linear response solvent model.[40,41] The use of semiempirical Hamiltonians allows NEXMD to simulate the dynamics of organic conjugated molecules on the order of hundreds of atoms and for time scales up to tens of picoseconds. Past developmental versions of NEXMD have been used to simulate the nonadiabatic dynamics of large systems such as dendrimers,[2,42−45] chlorophylls,[46−48] cycloparaphenylenes,[49] and conjugated macrocycles.[5] Integrating an implicit solvent model to the code is both an effort toward retaining the computational efficiency of NEXMD and incorporating the important solute−solvent interactions necessary for realistic modeling of molecular systems in contact with polarizable environments. Recently, adiabatic dynamics simulations have investigated solvatochromic shifts in the optical spectra of solvated oligo(*p*-phenylenevinylene) (PPVO) derivatives.[50] This work extends dynamics with implicit solvation to the nonadiabatic realm, where dynamical excited state properties are calculated in order to study their dependence on donor−acceptor functionalization and solvent polarity. Herein, we address the importance of solvation on dynamics and introduce a comprehensive version of NEXMD capable of efficiently modeling solvated molecules.

2. COMPUTATIONAL DETAILS

2.1. Nonadiabatic EXcited-state Molecular Dynamics (NEXMD) Framework. The NEXMD software combines the collective electronic oscillator (CEO) method[51,52] with the semiempirical quantum chemistry (SQM) package from AmberTools.[53] The CEO approach can be thought of as a generalization of the random phase approximation (RPA) applied to a range of mean field theories such as Hartree−Fock or Kohn−Sham DFT. NEXMD uses the CEO method to compute electronically excited states with RPA or configuration interaction with singles (CIS),[54] combined with the diverse set of semiempirical Hamiltonians that are available in SQM. At this level, the numerical costs of computing excited states are not substantially more demanding than ground state calculations.[55,56] Moreover, semiempirical Hamiltonians such as AM1[57] provide reasonably accurate ground state geometries and energies, heats of formation, vertical excitation energies, polarizabilities, and adiabatic excited state potential energy surfaces (PESs).[58−61] Optical and excited state properties of large systems with dense manifolds of interacting excited states may be computed as evidenced by successful application of this level of theory to systems such as polymers,[14,51,62] dendrimers,[63] light-harvesting complexes,[51] and carbon nanotubes.[64,65]

Energies and forces as well as nonadiabatic couplings are computed "on the fly" with nuclei evolving on native excited state PESs. Nonadiabatic transitions between electronic states are modeled with Tully's fewest-switches surface hopping (FSSH).[66] Other practical aspects of calculations that are carried out with NEXMD include but are not limited to (1) decoherence corrections built on top of FSSH to alleviate inconsistencies due to the classical treatment of nuclei,[67,68] (2) advanced algorithms for tracking trivial (unavoided) crossings between noninteracting states,[69] (3) implicit treatment of solvation including linear response,[40,41] state-specific,[40,41] and nonequilibrium models,[70] and (4) "on-the-fly" limiting to essential excited states that are needed to sufficiently propagate the electronic Schrödinger equation.[71] The latter functionality significantly reduces computational time by eliminating the calculation of unnecessary excited states and nonadiabatic couplings. More detail on the governing theory that is implemented in developmental versions of NEXMD can be found in refs 15 and 16. Full description of the NEXMD software such as structure, use, and benchmarks will be reported elsewhere, along with a public release of the code.

For the purposes of this paper, we focus on NEXMD's functionality of modeling implicit solvation—specifically, linear response solvation following the theoretical formalism reported in ref 40. Dynamics are coupled to the conductor-like polarizable continuum model (CPCM) from the SQM code using a standard tessellation scheme for cavity discretization.[72,73] Solvent response is related to the induced polarization with coefficient given by $f(\epsilon) = (\epsilon - 1)/\epsilon$, where ϵ is the dielectric constant of the solvent.[72,73] The surface charge distribution at the solute−solvent boundary produces an electrostatic potential which is added to the solute's Hamiltonian. This term accounts for the interaction of the solute's electrons and nuclei with the induced polarization charge. In order to properly simulate nonadiabatic dynamics, solvent effects are also included in the derivative coupling vectors:

$$\mathbf{d}_{\alpha\beta} = \frac{\langle \phi_\alpha(\mathbf{r};\,\mathbf{R})|\nabla_{\mathbf{R}} H|\phi_\beta(\mathbf{r};\,\mathbf{R})\rangle}{E_\beta - E_\alpha} \tag{1}$$

where H is the electronic Hamiltonian, parametrized by nuclear configuration, and contains a term for the solute−solvent interaction: $H = H_{vac} + H_{sol}$. The adiabatic eigenvectors and eigenvalues of H are $|\phi\rangle$ and E, respectively.

CPCM approximates PCM and treats the solvent as a conductor which simplifies numerical integration of Poisson's equation at the solute−solvent boundary. The coefficient of polarization $f(\epsilon)$ is an artificial function that ensures modeling of a solvent with a finite dielectric constant as opposed to a perfect conductor with an infinite dielectric constant. Nevertheless, CPCM has successfully reproduced experimental results.[73]

2.2. Studied PPVO Derivatives. *p*-Phenylenevinylene (PPV) is a prototype conjugated polymer with potential use in optoelectronic devices due to its rich electronic and optical properties as well as synthetic flexibility.[74−84] The PPVO derivatives (Figure 1) are molecular chromophores with

DOI: 10.1021/acs.jctc.8b00103
J. Chem. Theory Comput. 2018, 14, 3955−3966

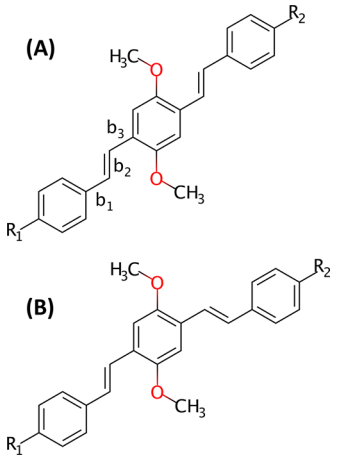

Figure 1. Chemical structures of PPVO derivatives. (A) and (B) are two different conformations. {$\mathbf{R}_1$, $\mathbf{R}_2$} are {H, H}, {H, NO_2}, and {NH_2, NO_2}. Bond lengths defined by b_1, b_2, and b_3 will be used to calculate bond length alternation (BLA) between the adjacent carbon−carbon atoms connecting the aromatic rings. BLA will be discussed in section 3.7.

tunable emission energies ranging across the optical spectrum.[85,86] In our simulations, we use the following three oligomers: unsubstituted {H, H}, substitution with an acceptor {H, NO_2}, and substitution with a donor−acceptor {NH_2, NO_2}. These molecules can adapt two distinct asymmetric and symmetric conformations as illustrated in Figure 1, parts A and B, respectively.

These molecules were chosen mainly because of their varying degrees of polarizability as a result of chemical substitution.[87] The calculated ground state dipole moments $|\vec{\mu}_{gg}|$ vary between 1.5−2.0, 6.8−7.9, and 8.4−9.6 D in {H, H}, {H, NO_2}, and {NH_2, NO_2}, respectively. The lower and upper bounds of each range correspond to $|\vec{\mu}_{gg}|$ with $\epsilon = 1$ and $\epsilon = 20$, respectively. The dipole moment progressively increases from apolar to polar molecules. Thus, we expect to see differences in the calculated excited state properties due to differences in their respective solute−solvent interactions.

2.3. Nonadiabatic Dynamics Simulations. The protocol taken to model nonadiabatic dynamics have been reported,[16] but for the sake of completeness, we summarize the steps here as well. A more detailed procedure is available in the Supporting Information. All molecular geometries were optimized using AM1 in NEXMD and then evolved adiabatically on their respective ground states for several nanoseconds with a 0.50 fs time step in a Langevin thermostat set to 300 K and a friction parameter of 20 ps^{-1}. Snapshots were taken throughout the equilibrated ground state trajectories of both conformers (Figure 1) which constitute inputs to excited state modeling. In our simulations, 80% of initial geometries used for nonadiabatic trajectories were sampled from the ground state trajectories of the asymmetric conformations of Figure 1A, while the other 20% were sampled from the other ground state trajectories with the symmetric conformations of Figure 1B. These proportions are approximate Boltzmann populations determined from total energies of the ground state optimized structures. [Absolute energy differences between the ground state optimized asymmetric and symmetric conformations of these molecules using the AM1 Hamiltonian range from 0.045 to 0.063 eV. For the sake of simplicity, we used the same proportions of asymmetric (80%) and symmetric (20%) conformations for the dynamical ensembles of the three PPVO molecules.]

Single-point calculations at ground state geometries were performed to determine excited state energies and oscillator strengths. Oscillator strengths were broadened with a Gaussian-shaped Franck−Condon window at the excitation energies with an empirical standard deviation of 0.15 eV. A theoretical absorption spectrum of each molecule was then calculated as an average over all the individual absorption spectra of its sampled ground state conformations. Emission spectra were also simulated to calculate Stokes shifts and compare them to experimental data. Similar to the procedure carried out for absorption, a single trajectory for each molecule evolved adiabatically on the first excited state S_1 for a few nanoseconds. Following thermal equilibration, geometries were sampled throughout these trajectories and single-point calculations determined $S_1 \rightarrow S_0$ emission energies and oscillator strengths.

Ground state snapshots (i.e., coordinates and velocities) were used as the initial conditions for nonadiabatic trajectories. Each trajectory was prepared in an optically allowed electronic excited state in the vicinity of the chosen photoexcitation energy. The initial excited state of each trajectory was chosen according to the absorption spectrum of its sampled ground state geometry such that states with larger oscillator strengths were more populated than those with lower oscillator strengths. This procedure composes a photoexcited wave packet sampling the phase space of nuclear configurations accessible at room temperature. Nonadiabatic trajectories evolved for 1 ps in length with a 0.10 fs classical time step (nuclei) and a 0.02 fs quantum time step (electrons) in the same Langevin thermostat as the ground state trajectories. Whenever FSSH signaled for a hop to occur, the electronic wave function was instantaneously collapsed onto the target state following the transition, thereby incorporating the appropriate decoherence correction.[67] Trivial crossings were also accounted for using a method developed and tested within the NEXMD framework.[69] In order to guarantee statistical convergence, each ensemble was comprised of 635 trajectories. A range of solvents from low to high polarity were modeled with $\epsilon = \{1, 2, 5, 20\}$.

2.4. Natural Transition Orbitals (NTOs) and Transition Density (TD) Analysis. Excitonic states of these π-conjugated oligomers have strong multireference character. Due to strong mixing, visualizing these excitations in terms of molecular orbitals does not provide useful information. A more useful analysis of the excited states was carried out by transforming molecular orbitals to natural transition orbitals (NTOs). By generating NTOs, the hole and electron wave functions were visualized and the ground to excited state transition characters were more accurately assigned as $\pi \rightarrow \pi^*$, charge transfer, etc. These holes and electrons come in pairs, where the relative weight of each pair are excitation amplitudes in the NTO basis. NTOs were calculated in the Gaussian 09[88] software, and images showing NTOs were obtained with the Visual Molecular Dynamics (VMD) software.[89]

Evolution of the excitonic wave function was tracked by changes in the spatial localization of the transition density (TD). Diagonal elements of the single-electron TD matrices

$$(\rho^{ge})_{mm}(t) \equiv \langle \phi_e(t)|c_m^\dagger c_m|\phi_g(t)\rangle \tag{2}$$

represent changes in the electronic density in an atomic orbital (AO) when undergoing a ground (g) to excited state (e) transition, where $c_m^\dagger$ and c_m are Fermi creation and annihilation

DOI: 10.1021/acs.jctc.8b00103
J. Chem. Theory Comput. 2018, 14, 3955−3966

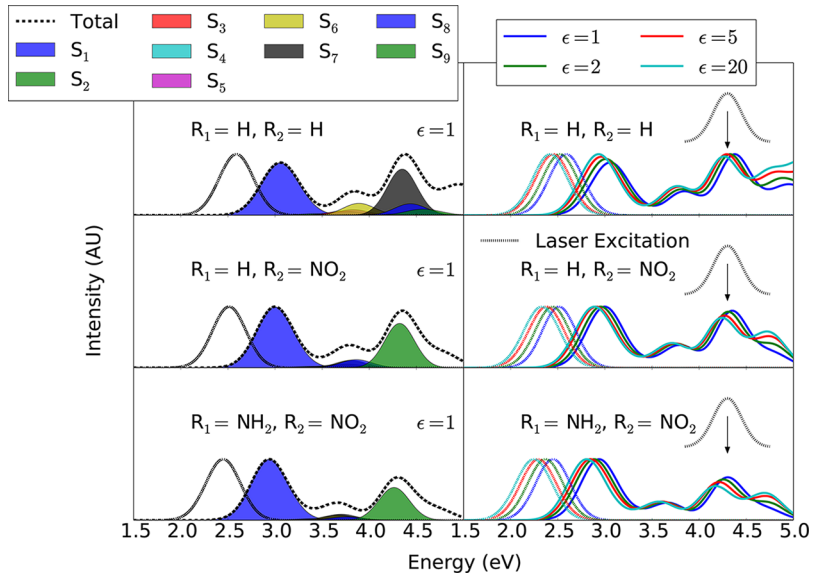

Figure 2. Calculated linear optical absorption spectra in arbitrary units (AU). Left panels show the spectra of the three molecules with $\epsilon = 1$. Both the individual states and the total absorption are shown. The dotted line shows the emission peak from S_1. Right panels show the total absorption of each molecule in four solvent environments with $\epsilon = \{1, 2, 5, 20\}$. The dotted lines show emission peaks from S_1. Each spectrum is normalized by its maximum absorption/emission intensity. Also shown in the right panels are the laser excitations at 4.30 eV with 0.15 eV line widths which mimic the initial excitation for nonadiabatic dynamics into high-energy absorption bands.

operators, respectively; m refers to the AO basis function.[90] Evolution of a TD matrix contains information regarding charge density fluctuations and spatial localization of excitations in time.[43,69,91,92] The fraction of TD localized on a molecular fragment is defined as the sum of all its atomic contributions.[93] For the purposes of this study, each molecule was divided into two fragments and the normalized probability distribution of the TD on each fragment (P_F) was calculated using

$$P_F = \frac{\sum_i^{\{N_F\}} |\xi_{ii}|}{\sum_j^{\{N\}} |\xi_{jj}|} \tag{3}$$

where ξ_{nn} is TD on the nth atom, $\{N_F\}$ are the atoms associated with the F fragment, and $\{N\}$ are all atoms of the molecule.[51] ξ is a $N \times N$ *reduced* TD matrix where diagonal elements ξ_{nn} are determined by summing the contributions of TD (ρ_{mm} of eq 2) from all AO basis functions associated with the nth atom.

In addition to describing the spatial localization of excitations with P_F, we also measure exciton localization L_D. The latter is defined as the inverse participation ratio associated with the distribution of populations[51]

$$L_D = \left(\sum_n P_n^2 \right)^{-1} \tag{4a}$$

$$P_n = \frac{|\xi_{nn}|}{\sum_j^{\{N\}} |\xi_{jj}|} \tag{4b}$$

For a localized excitation, $L_D \sim 1$, and for a delocalized excitation, $L_D \sim N$. Calculating L_D is a simple way of determining the localization/delocalization of molecular excitations as a function of chemical substitution and solvent polarity.

3. RESULTS AND DISCUSSION

3.1. Optical Spectra and Initial Excitation. The first step to modeling photoinduced dynamics is photoexcitation into optically allowed electronic states. The left panels of Figure 2 show the calculated absorption spectra of the three molecules with $\epsilon = 1$, where contributions of the individual excited states (S_1–S_9) are delineated. Three peaks are predicted within the optical window of interest, the locations of which do not vary by more than 0.20 eV across the three molecules. The right panels of Figure 2 show the integral spectrum of each molecule in the four solvent environments. The spectra shift toward lower energy as ϵ increases due to stabilization of the excited states relative to the ground state caused by the induced polarization (solvatochromic shifts). These shifts are within 0.30 eV. In order to study nonadiabatic dynamics through multiple excited states, the molecules were photoexcited at the high-energy peak. The laser excitation energy was a Gaussian-shaped pulse in the energy domain with a mean of 4.30 eV and an empirical line width parameter (standard deviation) of 0.15 eV (Figure 2).

A calculated absorption spectrum was compared to an experimental spectrum from the literature in order to support the use of NEXMD's level of theory for calculating excited states. The calculated spectrum of {H, H} is red-shifted relative to the experimental spectrum of PPV3[94] by about 0.20 eV, but the Stokes shift (which is approximately 0.5 eV) is in excellent agreement (Figure S1). This comparison between {H, H} and PPV3 is valid since the methoxy groups connected to the central benzene ring do not contribute to the optical excitation based on NTO analysis (discussed below). While the absolute excitation energies are slightly red-shifted compared to experiment, relative energy given by the Stokes shift is described well at the semiempirical level of theory. Similarly, nonradiative relaxation also depends on energy gaps, and therefore these results give us confidence in using NEXMD for studying qualitative differences in the dynamics due to functionalization and solvent polarity.

DOI: 10.1021/acs.jctc.8b00103
J. Chem. Theory Comput. 2018, 14, 3955−3966

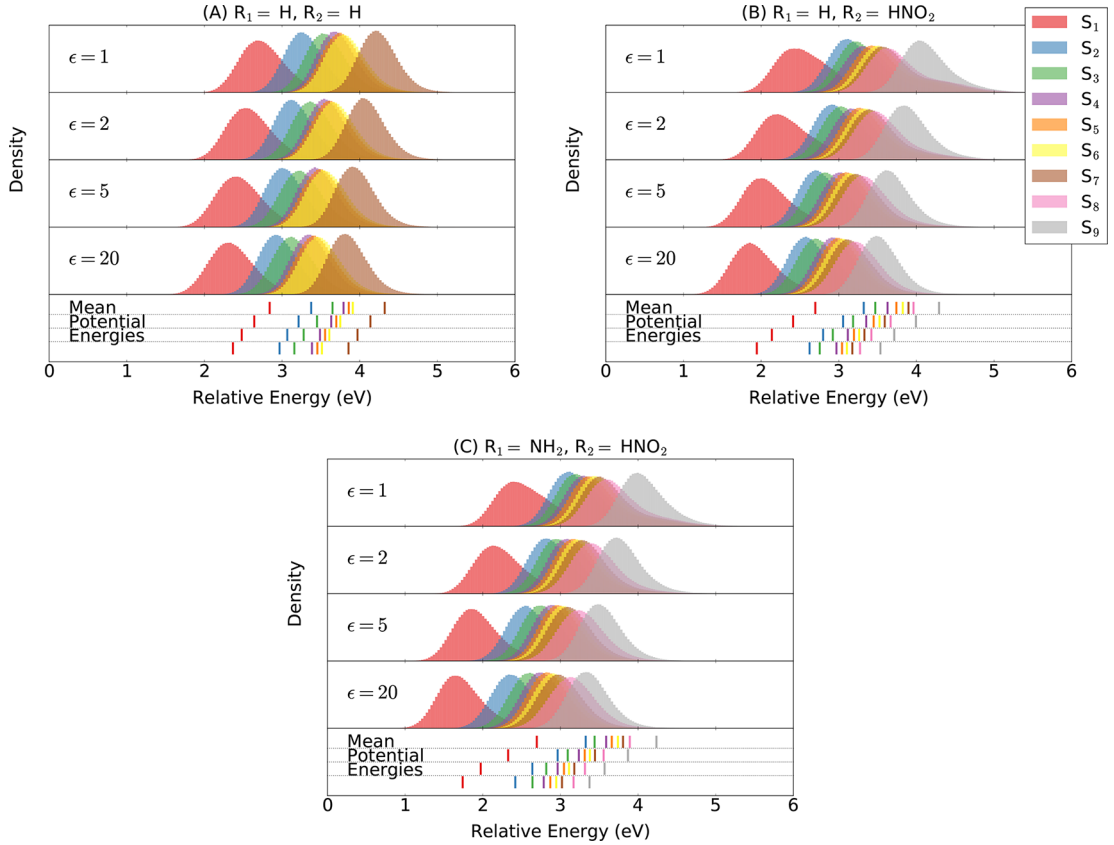

Figure 3. Histograms of the PESs over the entire 1 ps ensemble of trajectories with ϵ = {1, 2, 5, 20}. PESs of each molecule were shifted by their mean ground state energies with ϵ = 1. The maximum PES shown for each molecule corresponds to the optically excited state at 4.30 eV. The bottom panel of each subfigure shows mean PESs averaged over all time steps and trajectories.

The molecules of this study have different partial charge transfer character and are a test bed for investigating the effects of functionalization in different solvent environments. Transitions are independent of molecular conformations across all ground state dynamical data, and therefore we only present NTOs of S_1 (Table S1) and the optically excited state (Table S2) of the three molecules in their ground state optimized geometries with ϵ = 1. For {H, H}, the transition to the optically excited state has $\pi \rightarrow \pi^*$ character localized on the aromatic rings. Similar $\pi \rightarrow \pi^*$ transitions occur in {H, NO_2}, but unlike {H, H} which is an unsubstituted symmetric molecule, {H, NO_2} favors charge transfer toward the NO_2. Similarly, {NH_2, NO_2} also shows significant charge transfer from NH_2 to NO_2. The main transitions in all molecules are $\pi \rightarrow \pi^*$, but NTOs illustrate how charge transfer character can be controlled by chemical substitution. This is also reflected in the difference of dipole moments in the ground and excited states $\langle|\vec{\mu}_{ee} - \vec{\mu}_{gg}|\rangle$ which progressively increases from the apolar to polar molecules and varies from approximately 0.4, to 1.1, to 2.4 D across all dynamical simulations with ϵ = 1. The excited states used to calculate μ_{ee} are those that contribute most to the absorption peaks at 4.30 eV, which are S_7 for {H, H} and S_9 for {H, NO_2} and {NH_2, NO_2} (Figure 2).

3.2. Potential Energy Surfaces. Excited state dynamics depend on the topology of potential energy surfaces (PESs). Figure 3 shows solvatochromic shifts when PESs are histogrammed over all time steps and trajectories. To show relative differences in excited state energies as a function of ϵ, the PESs of each molecule were shifted by their mean ground state energies with ϵ = 1. As a consequence of the electrostatic interaction at the solute−solvent boundary, these shifts increase in the order {H, H}, {H, NO_2}, and {NH_2, NO_2}. For {H, H}, $\langle E_1\rangle(\epsilon) - \langle E_0\rangle(\epsilon{=}1)$ = 2.79 at ϵ = 1 and 2.29 at ϵ = 20, resulting in an overall shift of 0.50 eV. For {H, NO_2} and {NH_2, NO_2}, these shifts are 2.56 − 1.80 = 0.76 eV and 2.54 − 1.59 = 0.95 eV, respectively. Increasing solvent polarity stabilizes the energy levels and the degree of stabilization depends on donor−acceptor groups, where more polar molecules (i.e., {H, NO_2} and {NH_2, NO_2}) are further stabilized in more polar solvents.

3.3. Excited State Populations and Lifetimes. Figure 4 shows the lifetimes of electronic excitations. The initial excitation (black curve) fully decays in about 500 fs and rapidly transfers population through the intermediate states. The S_1 population was fit to the expression $A - B\exp(-kt)$, where k is the relaxation rate and t is time (Figure 4D). Relaxation rates of {H, H} do not strongly depend on solvent polarity since the molecule is weakly polarizable. In contrast, relaxation rates of the polar molecules do depend on solvent polarity.

Relaxation dynamics to S_1 are described by the energy gaps between excited states, $E_{ji} = E_j - E_i$. The gaps of {H, H} are larger than those of {H, NO_2} and {NH_2, NO_2} (Figure 3); nonadiabatic couplings[95] (eq 1) are larger in the polar molecules, leading to faster relaxation (Figure 4D). In regards to changes due to solvent polarity, energy gaps can either increase or decrease (Figure S2). [The number of gaps that fell below 0.1 eV was recorded (Figure S3). This value was chosen because the majority of hops occurred below this threshold.] The frequency of small energy gaps in {H, NO_2} generally

DOI: 10.1021/acs.jctc.8b00103
J. Chem. Theory Comput. 2018, 14, 3955−3966

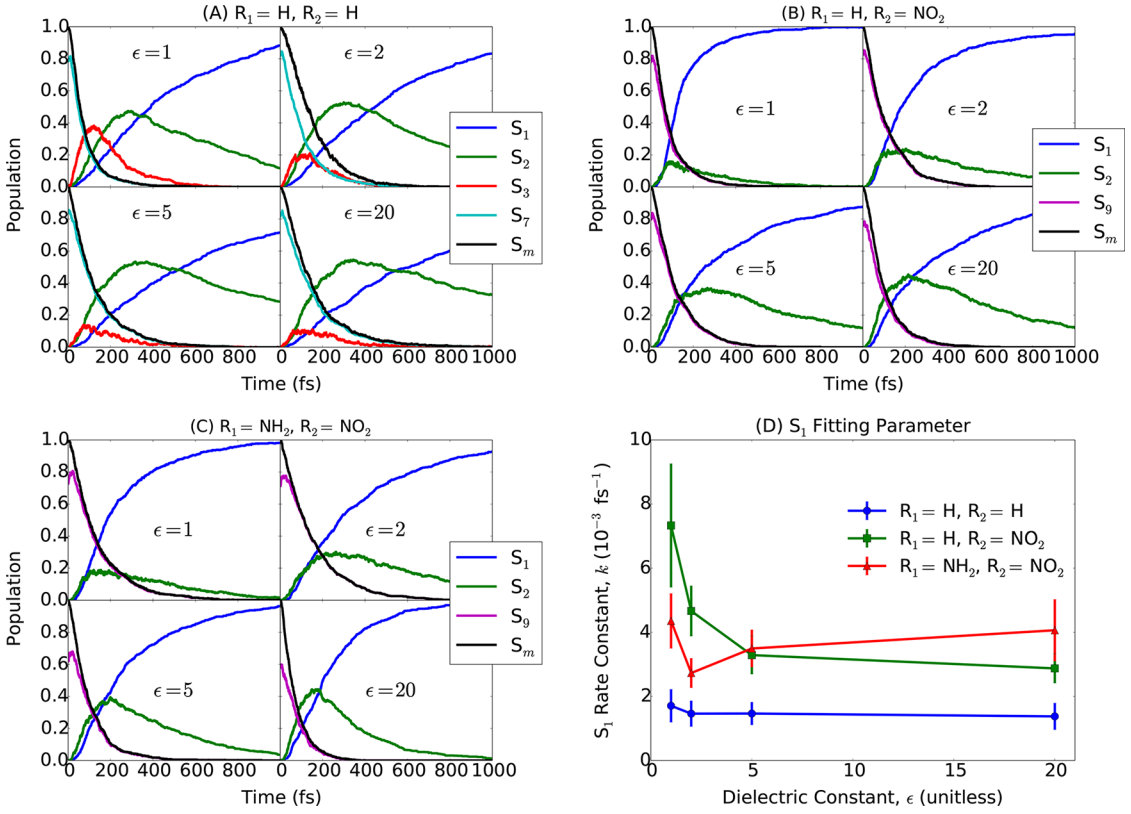

Figure 4. Excited state populations of (A) {H, H}, (B) {H, NO_2}, and (C) {NH_2, NO_2}, respectively. Each subpanel of (A)−(C) shows excited state populations in one of the solvent environments with ϵ = {1, 2, 5, 20}. Populations labeled with S_m are comprised of all states that are excited by the initial laser excitation at 4.30 eV. (D) Relaxation rates to S_1 determined by fitting S_1 populations to $A - B\exp(-kt)$. Error bars are ±one standard deviation in the associated fit.

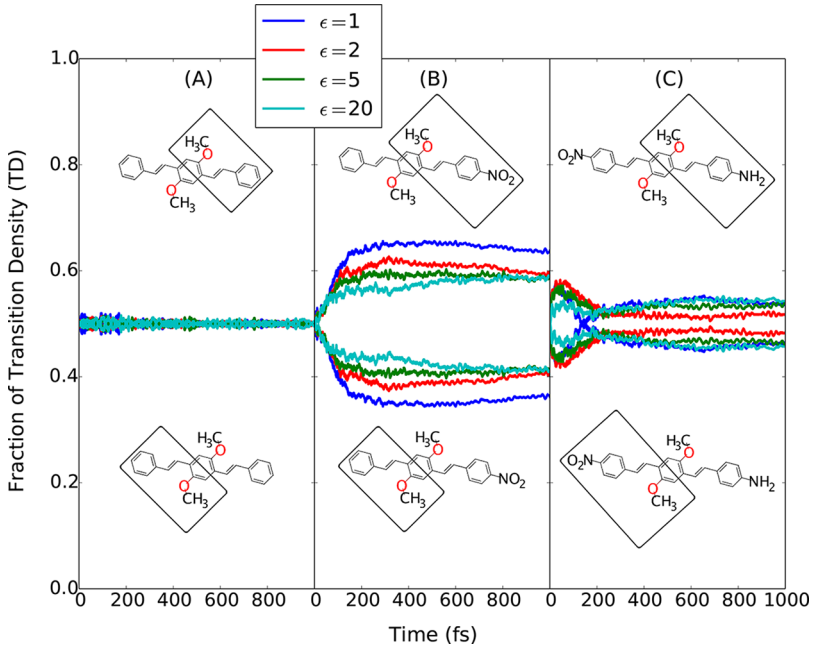

Figure 5. Fraction of transition density (TD) on specified (boxed) molecular fragments as a function of time. Asymmetric conformations of the molecules are shown for visualization, but the TDs of asymmetric and symmetric conformations are contained in the averaged results.

decreases with ϵ, thus explaining the monotonic decrease in k (Figure 4D). In contrast, the E_{32} gap of {H, H} decreases with increasing ϵ, and explains the decrease in S_3's population in more polar solvents (Figure 4A)— the $S_3 \rightarrow S_2$ transition becomes more easily accessible. The E_{98} gap of {NH_2, NO_2} fluctuates non-monotonically with ϵ (Figure S3) and correlates to changes seen in the S_1 population (Figure 4D). All these examples are given to highlight the effect of solvation on

DOI: 10.1021/acs.jctc.8b00103
J. Chem. Theory Comput. 2018, 14, 3955−3966

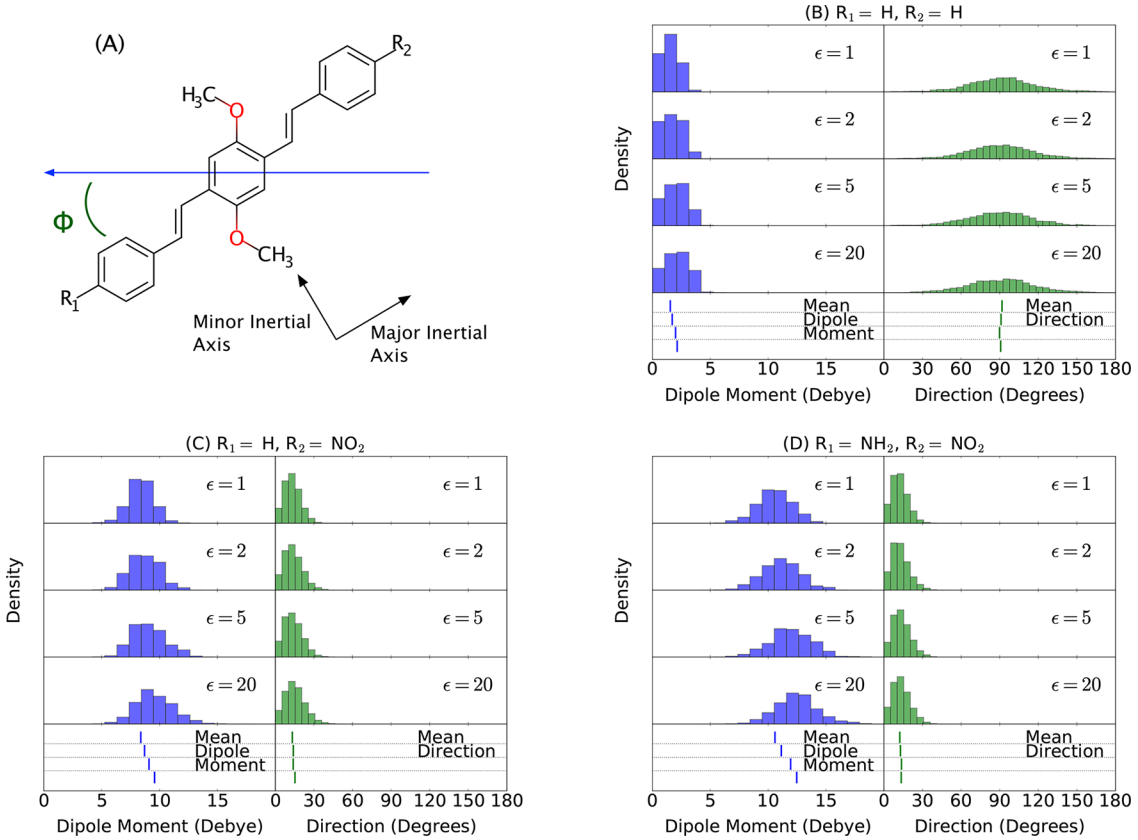

Figure 6. (A) Schematic labeling the relative direction of the permanent excited state dipole moment. The left panels of (B)−(D) show histograms of the magnitude of the dipole moment over all time steps and trajectories in four different solvent environments with ϵ = {1, 2, 5, 20}. The right panels of (B)−(D) show directions of the dipole moment, in similar format as the left panel. The bottom-most panels show the mean magnitudes and directions of the dipole moments, respectively.

relaxation as a result of changes in energy gaps. The degree to which an excited state is affected by solvation depends on its polarizability and charge transfer character (discussed in section 3.5). In summary, we find that relaxation to S_1 occurs on a 590−730, 140−350, and 230−370 fs time scale (k^{-1}) in {H, H}, {H, NO_2}, and {NH_2, NO_2}, respectively (Table S3). The range of each time scale refers to the effect of the different solvent environments.

3.4. Transition Density (TD) Analysis. Evolution of the excitonic wave function was qualitatively tracked by changes in spatial localization of the TD. Each molecule was split into two fragments, and the fraction of TD on each fragment was calculated with eq 3. In {H, H}, the excitation is split evenly on both fragments throughout the dynamics and is roughly independent of ϵ (Figure 5A). Both properties are expected since the molecule is symmetric and lacks electron donating and withdrawing groups. In {H, NO_2} at ϵ = 1, the excitation starts out evenly distributed and then transfers toward the NO_2 (Figure 5B); the exciton becomes more localized as trajectories evolve due to the electron withdrawing character of NO_2 by induction and resonance. In {NH_2, NO_2}, the excitation slightly favors the NH_2 fragment at initial time (Figure 5C), in agreement with NTOs of the optically excited state (Table S2). The excitation transfers toward the NO_2 and the fraction transferred decreases as ϵ increases similar to that observed in {H, NO_2} (Figure 5B), but to a lesser extent.

The spatial distribution of the TD is a consequence of the electron withdrawing or donating character of the functional groups. Both of the polar molecules are functionalized with NO_2, but the fraction of TD localized on the fragment containing NO_2 is larger in {H, NO_2} than in {NH_2, NO_2} (Figure 5). The NO_2 group decreases electron density on the ring through an electron withdrawing effect. This effect occurs in both molecules, but in the case of {NH_2, NO_2}, the NH_2 group also increases electron density on the adjacent aromatic ring through an electron donating effect. As a result, the excitation is more delocalized in {NH_2, NO_2}.

In regards to trends observed due to solvent polarity, the TD on each fragment of both molecules becomes more like the other as ϵ increases, resulting in a more delocalized ground to excited state transition. This effect is a consequence of functionalization along the major inertial axis, giving rise to relatively large dipole moments. But since dipole moments are large, an increase in ϵ only slightly affects the distribution of charge density and the fraction of TD on each fragment (Figure 5). This is more so the case for {NH_2, NO_2} than it is for {H, NO_2}.

A brief discussion of TD as a function of individual excited states and solvent polarities is available in Supporting Information (Figure S4).

3.5. Excited State Dipole Moments. Figure 6 shows histograms of excited state dipole moments. The dipoles of {H, H} are smaller in magnitude than those of {H, NO_2} and {NH_2, NO_2}. The relative direction also changes from being along the minor inertial axis (Figure 6A) in the apolar molecule (Figure 6B) to being nearly parallel along the major inertial axis in the polar molecules (Figure 6C,D) as a result of chemical substitution. Dipole magnitudes increase as ϵ increases and vary

DOI: 10.1021/acs.jctc.8b00103
J. Chem. Theory Comput. 2018, 14, 3955−3966

in the ranges 1.5−2.1, 8.4−9.6, and 10.6−12.5 D in the three molecules, respectively. The dipole moments of {H, NO_2} and {NH_2, NO_2} also show small changes in magnitude within the first 200 fs, indicative of charge transfer character (Figure S5). A brief discussion on charge transfer states is available in the Supporting Information (Figure S6).

Dipole moments computed with NEXMD can be validated by considering the inertial axis along which they are oriented. Dipoles vary from approximately 2 D in {H, H} to 12 D in {NH_2, NO_2}; a ratio of 6 is in approximate agreement with the length scales of the major and minor inertial axes for these molecules.

3.6. Exciton Localization. A measure of exciton localization brings together the preceding analyses of TDs and excited state dipole moments. Figure 7 shows a scatter plot of

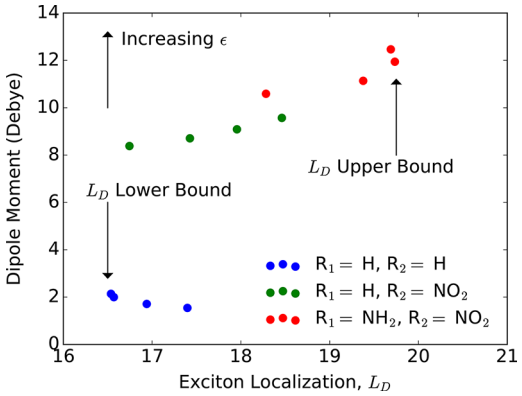

Figure 7. Excited state dipole moment versus exciton localization L_D. Each data point was computed as an average over all time steps and trajectories in the nonadiabatic ensembles.

dipole moment versus exciton localization (eq 4a) across all molecules and solvent polarities. The dipole moment of {H, H} is inversely related to L_D (shown in blue); an increase of the dipole moment along the minor inertial axis (Figure 6B) localizes the exciton, but only to a small extent due to the molecule's low degree of polarizability. Once $\epsilon > 5$, L_D saturates, thus defining a lower bound within this set of molecules. In the cases of {H, NO_2} and {NH_2, NO_2}, the excitation is more delocalized since functionalization and dipole moments are aligned along the major inertial axis. For {H, NO_2}, L_D gradually increases with ϵ, suggesting that the spatial extent of the excitation is more variable as a function of solvent polarity (shown in green). This is not the case for {NH_2, NO_2}, which experiences an upper bound on L_D at $\epsilon > 5$ (shown in red); substitution with donor−acceptor groups attached at the ends of the molecule delocalizes the excitation so that even a small increase in ϵ maximizes the size of the exciton. $L_D^{upper} - L_D^{lower}$ is relatively small in these molecules (as it should be for small π-conjugated structures), but this analysis uncovers qualitative differences among the excitations due to functionalization and solvent polarity.

There is a connection between the results of Figure 7 and relaxation time scales of Figure 4D. Although {NH_2, NO_2} is more polar than {H, NO_2}, its exciton size does not vary as much with ϵ. Similarly, relaxation time scales of {NH_2, NO_2} are less dependent on solvent polarity compared to {H, NO_2}. In other words, the relaxation rate of the more polar molecule {NH_2, NO_2} is less affected by the presence of more polar solvents since its exciton size is already close to maximum. In the opposite direction, {H, H} is the least polar molecule; exciton size and relaxation time scales are changed only slightly due to the presence of more polar solvents. The simulations of this paper use implicit solvation, and therefore more work is needed to study this effect in the context of explicit solvation.

3.7. Bond Length Alternation (BLA). Bond length alternation (BLA) between adjacent carbon−carbon atoms, $[(b_1 + b_3)/2] - b_2$ (Figure 1A), was calculated to quantify the dependence of chemical substitution and solvent polarity on structural relaxation. BLAs were calculated between both outer aromatic rings and the central ring independently (Figure 8).

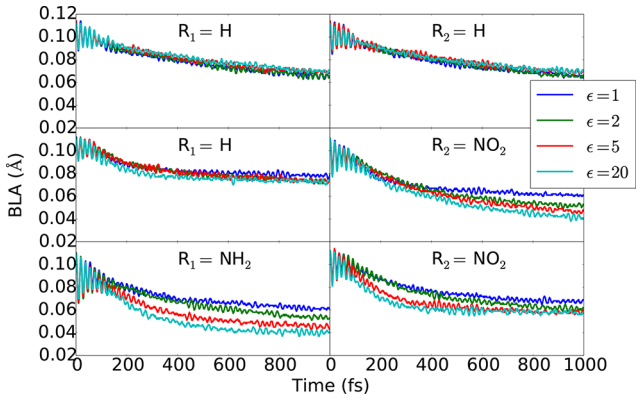

Figure 8. Bond length alternation (BLA) as a function of time. Each row represents a different molecule. The left and right panels show the BLA on the side of the molecule containing $\mathbf{R}_1$ and $\mathbf{R}_2$, respectively. Coherent oscillations in the BLA are observed within the first 100 fs, which shows the transfer of optical energy to nuclear vibrational modes and the ultrafast relaxation on the femtosecond time scale.

BLA decreases in time, thus verifying that it is greater in the ground state than in the excited state.[14,15] As expected, BLA does not vary as a function of solvent polarity in the apolar molecule, but does in the polar molecules.

The varying dependence of BLA with solvent polarity is a consequence of zwitterions.[96] In {H, NO_2}, BLA decreases with increasing ϵ on the side containing NO_2. A zwitterion of {H, NO_2} shows bond order on the NO_2 side changing from single to double bond character and vice versa (Figure S7). For the same structure, bond character on the H side is unaffected, in agreement with calculations (middle left panel of Figure 8). In contrast, as a result of a zwitterion that flips bond character throughout the entire molecule (Figure S7), BLA of {NH_2, NO_2} decreases with increasing ϵ on both sides of the molecule (bottom panels of Figure 8). BLA is further reduced on the side containing NH_2, which is likely due to another zwitterion that exclusively flips bond order on the NH_2 fragment, leaving the NO_2 fragment unchanged (Figure S7).

BLA decreases as ϵ increases due to more solvent-stable resonance structures (zwitterions), where the contributions of single and double bond character become more alike. This is not the case for {H, H} since it lacks functional groups that can change the bond order of the adjacent carbon−carbon atoms. Both observations qualitatively agree with simple chemical expectations. This analysis not only conveys the dependence of chemical substitution and solvent polarity on structural relaxation but further validates calculations carried out with NEXMD.

3.8. Relative Computational Time. The linear response solvent model added very little computational overhead to the

DOI: 10.1021/acs.jctc.8b00103
J. Chem. Theory Comput. 2018, 14, 3955−3966

nonadiabatic simulations. CPU times were averaged over all trajectories of each ensemble computed with and without the solvent model at $\epsilon = 20$ and $\epsilon = 1$, respectively (Figure S8). [CPU times do not vary among simulations with $\epsilon \neq 1$.] The total CPU time increased by slightly less than 10%, which is mainly due to a 30% increase in the excited state calculation. But compared to the large computational cost of nonadiabatic couplings, this increase is relatively small—excited-state CPU time scales linearly with the number of excited states, while nonadiabatic couplings scale quadratically. Even the large computational expense of nonadiabatic couplings can be alleviated by reducing the number of computed couplings between states to a small fraction that are nearby in energy to the occupied state of the system.[71] In this way, numerical costs of nonadiabatic couplings become practically independent of the number of excited states.

4. CONCLUSIONS

Modeling solvation has obvious computational challenges due to the number of degrees of freedom in a solvent. Reducing the computational cost needed to model solvation while still capturing the effective solvent response is a desired attribute of solvated atomistic simulations. In this work, we have implemented and demonstrated the use of an implicit solvent model in the Nonadiabatic EXcited-state Molecular Dynamics (NEXMD) software.

The NEXMD software is an efficient framework for excited state modeling of large molecular systems. The code calculates electronically excited states at the time dependent Hartree–Fock (TD-HF) or configuration interaction with singles (CIS) level combined with a family of optimized semiempirical Hamiltonians. This level of theory, merged with improved surface hopping methodologies for electronic transitions, makes it feasible to simulate the nonadiabatic dynamics of molecules with sizes on the order of hundreds of atoms and for time scales up to tens of picoseconds. This is a signature property of the code enabling the simulation of large molecular systems where more elaborate ab initio approaches would be numerically prohibitive. This work introduced a version of NEXMD based on the semiempirical quantum chemistry (SQM) code from AmberTools,[53] which contains a diverse set of semiempirical Hamiltonians and a linear response conductor-like polarizable continuum model (CPCM).

Benchmarks of solvent effects against a test bed of push–pull (donor–acceptor) PPVO derivatives were meant to both validate the use of this CPCM for future studies seeking to utilize the code and determine the interplay of functionalization and solvent polarity on photoinduced nonadiabatic dynamics. Our results showed that solvation can change dynamic and static properties, where the dependence of solvent polarity is determined by molecular polarizability due to chemical substitution. In the case of the {H, H} oligomer, many of the calculated properties are less dependent on solvent polarity due to the molecule's low degree of polarizability. On the other hand, substitution with electron donating and withdrawing groups in {H, NO_2} and {NH_2, NO_2} change excited state lifetimes, exciton localization, and structural relaxation. For example, we established how functionalization and solvent polarity affect spatial confinement of molecular excitations (Figures 5 and 7) and evolution of structural parameters such as bond length alternation (BLA) (Figure 8). Of the many properties that were analyzed, a few followed the expected trends based on chemical and physical intuition such as stabilization of energy levels (Figure 3) and dependence of excited state dipole moments with solvent polarity (Figure 6). Others, however, such as changes in excited state lifetimes due to solvent-induced fluctuations in energy gaps (Figure 4), are evidence of the complex behavior that solvation can have on nonradiative relaxation. These results suggest that theoretical interpretations may be altered depending on whether the effects of solvation are strong. With an integrated implicit solvent model, the NEXMD software has further become an appealing framework for realistic modeling of the photoinduced nonadiabatic dynamics in a diverse set of solvated chemical systems.

This work both demonstrates an important extension to NEXMD's capabilities and sets the stage for other advanced features of the code. We have shown that CPCM modeling adds little numerical overhead to the simulations, thus presenting an efficient way to model solvent effects in extended systems. Our future work will include implementation of state-specific[40,41] and nonequilibrium[70] solvent models in the context of nonadiabatic dynamics. The use of these models is relevant since the dynamics following photoexcitation proceeds through many excited states and are generally out of equilibrium (i.e., the solute and solvent polarizations are not equilibrated with one another). However, more work is needed to determine how important such effects are on dynamics as they likely depend on the solute–solvent system of interest. Furthermore, an important property of the solvent model used for this study is that the coefficient of induced polarization goes as $(\epsilon - 1)/\epsilon$; solvent effects asymptotically decrease with increasing ϵ as evidenced by the relaxation time scales of Figure 4D. Whether high dielectric constants significantly change dynamics requires further investigation, which is why extending this work to explicit solvation is important. Indeed there has been an ongoing effort to introduce a QM/MM solvent model to NEXMD, as implemented in AmberTools. The goal is to evaluate implicit and explicit solvation on dynamics, and to assess the validity of each model based on chemical composition of the solute–solvent system.

■ ASSOCIATED CONTENT

Supporting Information

The Supporting Information is available free of charge on the ACS Publications website at DOI: 10.1021/acs.jctc.8b00103.

Detailed description of nonadiabatic dynamics modeling procedure. Comparison of theoretical and experimental optical absorption and emission spectra. NTOs of the first excited state (S_1) and the optically excited states at 4.30 eV. Energy gaps throughout the dynamics. Number of small energy gaps that fell below a 0.1 eV threshold throughout the dynamics. Exponential rate and time decay constants of fitted S_1 populations (Figure 4). Fraction of TD due to ground to excited state transitions as a function of individual excited states and ϵ. Excited state dipole moments as a function of time. Difference of dipole moments in the ground and excited states $|\vec{\mu}_{ee} - \vec{\mu}_{gg}|$ as a function of individual excited states and ϵ. Solvent-stable resonance structures (zwitterions). Relative CPU times of the nonadiabatic simulations. Comparison between semiempirical theory and TD-DFT for absorption spectra and ground and first excited state dipole moments (PDF)

DOI: 10.1021/acs.jctc.8b00103
J. Chem. Theory Comput. 2018, 14, 3955–3966

AUTHOR INFORMATION

Corresponding Author

*E-mail: serg@lanl.gov.

ORCID

Andrew E. Sifain: 0000-0002-2964-1923
Josiah A. Bjorgaard: 0000-0003-3679-2487
Tammie R. Nelson: 0000-0002-3173-5291
Brendan J. Gifford: 0000-0002-4116-711X
Oleg V. Prezhdo: 0000-0002-5140-7500
Sebastian Fernandez-Alberti: 0000-0002-0916-5069
Adrian E. Roitberg: 0000-0003-3963-8784
Sergei Tretiak: 0000-0001-5547-3647

Funding

The authors acknowledge support of the U.S. Department of Energy through the Los Alamos National Laboratory (LANL) LDRD Program. O.V.P. and A.E.S. acknowledge support of the U.S. Department of Energy, Grant DE-SC0014429.

Notes

The authors declare no competing financial interest.

ACKNOWLEDGMENTS

LANL is operated by Los Alamos National Security, LLC, for the National Nuclear Security Administration of the U.S. Department of Energy under Contract No. DE-AC52-06NA25396. This work was done in part at the Center for Nonlinear Studies (CNLS) and the Center for Integrated Nanotechnologies (CINT) at LANL. We also acknowledge the LANL Institutional Computing (IC) program for providing computational resources. A.E.S. thanks CNLS for their support and hospitality.

REFERENCES

(1) Rego, L. G.; Batista, V. S. Quantum Dynamics Simulations of Interfacial Electron Transfer in Sensitized TiO_2 Semiconductors. *J. Am. Chem. Soc.* **2003**, *125*, 7989−7997.

(2) Fernandez-Alberti, S.; Kleiman, V. D.; Tretiak, S.; Roitberg, A. E. Unidirectional Energy Transfer in Conjugated Molecules: The Crucial Role of High-Frequency C≡C Bonds. *J. Phys. Chem. Lett.* **2010**, *1*, 2699−2704.

(3) Akimov, A. V.; Neukirch, A. J.; Prezhdo, O. V. Theoretical Insights into Photoinduced Charge Transfer and Catalysis at Oxide Interfaces. *Chem. Rev.* **2013**, *113*, 4496−4565.

(4) Wang, L.; Long, R.; Prezhdo, O. V. Time-Domain Ab Initio Modeling of Photoinduced Dynamics at Nanoscale Interfaces. *Annu. Rev. Phys. Chem.* **2015**, *66*, 549−579.

(5) Alfonso Hernandez, L.; Nelson, T.; Gelin, M. F.; Lupton, J. M.; Tretiak, S.; Fernandez-Alberti, S. Interference of Interchromophoric Energy-Transfer Pathways in π-Conjugated Macrocycles. *J. Phys. Chem. Lett.* **2016**, *7*, 4936−4944.

(6) Goyal, P.; Hammes-Schiffer, S. Tuning the Ultrafast Dynamics of Photoinduced Proton-Coupled Electron Transfer in Energy Conversion Processes. *ACS Energy Lett.* **2017**, *2*, 512−519.

(7) Schultz, T.; Quenneville, J.; Levine, B.; Toniolo, A.; Martínez, T. J.; Lochbrunner, S.; Schmitt, M.; Shaffer, J. P.; Zgierski, M. Z.; Stolow, A. Mechanism and Dynamics of Azobenzene Photoisomerization. *J. Am. Chem. Soc.* **2003**, *125*, 8098−8099.

(8) Levine, B. G.; Martínez, T. J. Isomerization through Conical Intersections. *Annu. Rev. Phys. Chem.* **2007**, *58*, 613−634.

(9) Vincent, J. C.; Muuronen, M.; Pearce, K. C.; Mohanam, L. N.; Tapavicza, E.; Furche, F. That Little Extra Kick: Nonadiabatic Effects in Acetaldehyde Photodissociation. *J. Phys. Chem. Lett.* **2016**, *7*, 4185−4190.

(10) Nelson, T.; Bjorgaard, J.; Greenfield, M.; Bolme, C.; Brown, K.; McGrane, S.; Scharff, R. J.; Tretiak, S. Ultrafast Photodissociation Dynamics of Nitromethane. *J. Phys. Chem. A* **2016**, *120*, 519−526.

(11) Abuabara, S. G.; Rego, L. G.; Batista, V. S. Influence of Thermal Fluctuations on Interfacial Electron Transfer in Functionalized TiO_2 Semiconductors. *J. Am. Chem. Soc.* **2005**, *127*, 18234−18242.

(12) Torres, A.; Oliboni, R. S.; Rego, L. G. Vibronic and Coherent Effects on Interfacial Electron Transfer Dynamics. *J. Phys. Chem. Lett.* **2015**, *6*, 4927−4935.

(13) Nelson, T. R.; Fernandez-Alberti, S.; Roitberg, A. E.; Tretiak, S. Electronic Delocalization, Vibrational Dynamics and Energy Transfer in Organic Chromophores. *J. Phys. Chem. Lett.* **2017**, *8*, 3020.

(14) Tretiak, S.; Saxena, A.; Martin, R.; Bishop, A. Conformational Dynamics of Photoexcited Conjugated Molecules. *Phys. Rev. Lett.* **2002**, *89*, 097402.

(15) Nelson, T.; Fernandez-Alberti, S.; Chernyak, V.; Roitberg, A. E.; Tretiak, S. Nonadiabatic Excited-State Molecular Dynamics Modeling of Photoinduced Dynamics in Conjugated Molecules. *J. Phys. Chem. B* **2011**, *115*, 5402−5414.

(16) Nelson, T.; Fernandez-Alberti, S.; Roitberg, A. E.; Tretiak, S. Nonadiabatic Excited-State Molecular Dynamics: Modeling Photophysics in Organic Conjugated Materials. *Acc. Chem. Res.* **2014**, *47*, 1155−1164.

(17) Granström, M.; Petritsch, K.; Arias, A.; Lux, A.; Andersson, M.; Friend, R. Laminated Fabrication of Polymeric Photovoltaic Diodes. *Nature* **1998**, *395*, 257−260.

(18) Cao, Y.; Parker, I. D.; Yu, G.; Zhang, C.; Heeger, A. J. Improved Quantum Efficiency for Electroluminescence in Semiconducting Polymers. *Nature* **1999**, *397*, 414−417.

(19) Sirringhaus, H.; Kawase, T.; Friend, R.; Shimoda, T.; Inbasekaran, M.; Wu, W.; Woo, E. High-Resolution Inkjet Printing of All-Polymer Transistor Circuits. *Science* **2000**, *290*, 2123−2126.

(20) Brédas, J.-L.; Beljonne, D.; Coropceanu, V.; Cornil, J. Charge-Transfer and Energy-Transfer Processes in π-Conjugated Oligomers and Polymers: A Molecular Picture. *Chem. Rev.* **2004**, *104*, 4971−5004.

(21) Satishkumar, B.; Brown, L. O.; Gao, Y.; Wang, C.-C.; Wang, H.-L.; Doorn, S. K. Reversible Fluorescence Quenching in Carbon Nanotubes for Biomolecular Sensing. *Nat. Nanotechnol.* **2007**, *2*, 560−564.

(22) Brédas, J.-L.; Norton, J. E.; Cornil, J.; Coropceanu, V. Molecular Understanding of Organic Solar Cells: The Challenges. *Acc. Chem. Res.* **2009**, *42*, 1691−1699.

(23) Brédas, J.-L.; Silbey, R. Excitons Surf Along Conjugated Polymer Chains. *Science* **2009**, *323*, 348−349.

(24) Collini, E.; Scholes, G. D. Coherent Intrachain Energy Migration in a Conjugated Polymer at Room Temperature. *Science* **2009**, *323*, 369−373.

(25) Brédas, J.-L.; Cornil, J.; Beljonne, D.; Dos Santos, D. A.; Shuai, Z. Excited-State Electronic Structure of Conjugated Oligomers and Polymers: A Quantum-Chemical Approach to Optical Phenomena. *Acc. Chem. Res.* **1999**, *32*, 267−276.

(26) Spano, F. C. Emission from Aggregates of Oligo-phenylene vinylenes: A Recipe for Superradiant H-aggregates. *Chem. Phys. Lett.* **2000**, *331*, 7−13.

(27) Kistler, K. A.; Matsika, S. Solvatochromic Shifts of Uracil and Cytosine using a Combined Multireference Configuration Interaction/Molecular Dynamics Approach and the Fragment Molecular Orbital Method. *J. Phys. Chem. A* **2009**, *113*, 12396−12403.

(28) Isborn, C. M.; Gotz, A. W.; Clark, M. A.; Walker, R. C.; Martínez, T. J. Electronic Absorption Spectra from MM and Ab initio QM/MM Molecular Dynamics: Environmental Effects on the Absorption Spectrum of Photoactive Yellow Protein. *J. Chem. Theory Comput.* **2012**, *8*, 5092−5106.

(29) Goyal, P.; Schwerdtfeger, C. A.; Soudackov, A. V.; Hammes-Schiffer, S. Nonadiabatic Dynamics of Photoinduced Proton-Coupled Electron Transfer in a Solvated Phenol-Amine Complex. *J. Phys. Chem. B* **2015**, *119*, 2758−2768.

DOI: 10.1021/acs.jctc.8b00103
J. Chem. Theory Comput. 2018, 14, 3955−3966

(30) Lin, Y.-l.; Gao, J. Solvatochromic Shifts of the n→ π^* Transition of Acetone from Steam Vapor to Ambient Aqueous Solution: A Combined Configuration Interaction QM/MM Simulation Study Incorporating Solvent Polarization. *J. Chem. Theory Comput.* **2007**, *3*, 1484−1493.
(31) Röhrig, U. F.; Frank, I.; Hutter, J.; Laio, A.; VandeVondele, J.; Rothlisberger, U. QM/MM Car-Parrinello Molecular Dynamics Study of the Solvent Effects on the Ground State and on the First Excited Singlet State of Acetone in Water. *ChemPhysChem* **2003**, *4*, 1177−1182.
(32) Gao, J. Energy Components of Aqueous Solution: Insight from Hybrid QM/MM Simulations using a Polarizable Solvent Model. *J. Comput. Chem.* **1997**, *18*, 1061−1071.
(33) Tawa, G. J.; Martin, R. L.; Pratt, L. R.; Russo, T. V. Solvation Free Energy Calculations using a Continuum Dielectric Model for the Solvent and Gradient-Corrected Density Functional Theory for the Solute. *J. Phys. Chem.* **1996**, *100*, 1515−1523.
(34) Martin, R. L.; Hay, P. J.; Pratt, L. R. Hydrolysis of Ferric Ion in Water and Conformational Equilibrium. *J. Phys. Chem. A* **1998**, *102*, 3565−3573.
(35) Cramer, C. J.; Truhlar, D. G. Implicit Solvation Models: Equilibria, Structure, Spectra, and Dynamics. *Chem. Rev.* **1999**, *99*, 2161−2200.
(36) Mennucci, B.; Cammi, R. *Continuum Solvation Models in Chemical Physics: From Theory to Applications*; John Wiley & Sons: Chichester, U.K., 2007.
(37) Mennucci, B. Polarizable Continuum Model. *WIREs: Comput. Mol. Sci.* **2012**, *2*, 386−404.
(38) Tomasi, J.; Mennucci, B.; Cammi, R. Quantum Mechanical Continuum Solvation Models. *Chem. Rev.* **2005**, *105*, 2999−3094.
(39) Scalmani, G.; Frisch, M. J.; Mennucci, B.; Tomasi, J.; Cammi, R.; Barone, V. Geometries and Properties of Excited States in the Gas Phase and in Solution: Theory and Application of a Time-Dependent Density Functional Theory Polarizable Continuum Model. *J. Chem. Phys.* **2006**, *124*, 094107.
(40) Bjorgaard, J. A.; Kuzmenko, V.; Velizhanin, K.; Tretiak, S. Solvent Effects in Time-Dependent Self-Consistent Field Methods. I. Optical Response Calculations. *J. Chem. Phys.* **2015**, *142*, 044103.
(41) Bjorgaard, J. A.; Velizhanin, K. A.; Tretiak, S. Solvent Effects in Time-Dependent Self-Consistent Field Methods. II. Variational Formulations and Analytical Gradients. *J. Chem. Phys.* **2015**, *143*, 054305.
(42) Fernandez-Alberti, S.; Kleiman, V. D.; Tretiak, S.; Roitberg, A. E. Nonadiabatic Molecular Dynamics Simulations of the Energy Transfer between Building Blocks in a Phenylene Ethynylene Dendrimer†. *J. Phys. Chem. A* **2009**, *113*, 7535−7542.
(43) Fernandez-Alberti, S.; Roitberg, A. E.; Kleiman, V. D.; Nelson, T.; Tretiak, S. Shishiodoshi Unidirectional Energy Transfer Mechanism in Phenylene Ethynylene Dendrimers. *J. Chem. Phys.* **2012**, *137*, 22A526.
(44) Soler, M. A.; Roitberg, A. E.; Nelson, T.; Tretiak, S.; Fernandez-Alberti, S. Analysis of State-Specific Vibrations Coupled to the Unidirectional Energy Transfer in Conjugated Dendrimers. *J. Phys. Chem. A* **2012**, *116*, 9802−9810.
(45) Galindo, J. F.; Atas, E.; Altan, A.; Kuroda, D. G.; Fernandez-Alberti, S.; Tretiak, S.; Roitberg, A. E.; Kleiman, V. D. Dynamics of Energy Transfer in a Conjugated Dendrimer Driven by Ultrafast Localization of Excitations. *J. Am. Chem. Soc.* **2015**, *137*, 11637−11644.
(46) Bricker, W. P.; et al. Non-Radiative Relaxation of Photoexcited Chlorophylls: Theoretical and Experimental Study. *Sci. Rep.* **2015**, *5*, 13625.
(47) Shenai, P. M.; Fernandez-Alberti, S.; Bricker, W. P.; Tretiak, S.; Zhao, Y. Internal Conversion and Vibrational Energy Redistribution in Chlorophyll *a*. *J. Phys. Chem. B* **2016**, *120*, 49−58.
(48) Zheng, F.; Fernandez-Alberti, S.; Tretiak, S.; Zhao, Y. Photoinduced Intra-and Intermolecular Energy Transfer in Chlorophyll *a* Dimer. *J. Phys. Chem. B* **2017**, *121*, 5331−5339.
(49) Adamska, L.; Nayyar, I.; Chen, H.; Swan, A. K.; Oldani, N.; Fernandez-Alberti, S.; Golder, M. R.; Jasti, R.; Doorn, S. K.; Tretiak, S. Self-Trapping of Excitons, Violation of Condon Approximation, and Efficient Fluorescence in Conjugated Cycloparaphenylenes. *Nano Lett.* **2014**, *14*, 6539−6546.
(50) Bjorgaard, J. A.; Nelson, T.; Kalinin, K.; Kuzmenko, V.; Velizhanin, K. A.; Tretiak, S. Simulations of Fluorescence Solvatochromism in Substituted PPV Oligomers from Excited State Molecular Dynamics with Implicit Solvent. *Chem. Phys. Lett.* **2015**, *631*−*632*, 66−69.
(51) Tretiak, S.; Mukamel, S. Density Matrix Analysis and Simulation of Electronic Excitations in Conjugated and Aggregated Molecules. *Chem. Rev.* **2002**, *102*, 3171−3212.
(52) Mukamel, S.; Tretiak, S.; Wagersreiter, T.; Chernyak, V. Electronic Coherence and Collective Optical Excitations of Conjugated Molecules. *Science* **1997**, *277*, 781−787.
(53) Case, D.; et al. *AMBER 2017*; University of California, San Francisco, 2017.
(54) Thouless, D. J. *The Quantum Mechanics of Many-Body Systems*; Courier Corp.: 2013.
(55) Chernyak, V.; Schulz, M. F.; Mukamel, S.; Tretiak, S.; Tsiper, E. V. Krylov-Space Algorithms for Time-Dependent Hartree-Fock and Density Functional Computations. *J. Chem. Phys.* **2000**, *113*, 36−43.
(56) Tretiak, S.; Isborn, C. M.; Niklasson, A. M.; Challacombe, M. Representation Independent Algorithms for Molecular Response Calculations in Time-Dependent Self-Consistent Field Theories. *J. Chem. Phys.* **2009**, *130*, 054111.
(57) Dewar, M. J.; Zoebisch, E. G.; Healy, E. F.; Stewart, J. J. Development and Use of Quantum Mechanical Molecular Models. 76. AM1: A New General Purpose Quantum Mechanical Molecular Model. *J. Am. Chem. Soc.* **1985**, *107*, 3902−3909.
(58) Tretiak, S.; Saxena, A.; Martin, R.; Bishop, A. CEO/Semiempirical Calculations of UV-Visible Spectra in Conjugated Molecules. *Chem. Phys. Lett.* **2000**, *331*, 561−568.
(59) Tretiak, S.; Saxena, A.; Martin, R.; Bishop, A. Collective Electronic Oscillator/Semiempirical Calculations of Static Nonlinear Polarizabilities in Conjugated Molecules. *J. Chem. Phys.* **2001**, *115*, 699−707.
(60) Meng, Z.; Dölle, A.; Carper, W. R. Gas Phase Model of an Ionic Liquid: Semi-Empirical and Ab Initio Bonding and Molecular Structure. *J. Mol. Struct.: THEOCHEM* **2002**, *585*, 119−128.
(61) Stewart, J. J. Comparison of the Accuracy of Semiempirical and Some DFT Methods for Predicting Heats of Formation. *J. Mol. Model.* **2004**, *10*, 6−12.
(62) Mukamel, S.; Takahashi, A.; Wang, H. X.; Chen, G. Electronic Coherence and Nonlinear Susceptibilities of Conjugated Polyenes. *Science* **1994**, *266*, 250−250.
(63) Tretiak, S.; Chernyak, V.; Mukamel, S. Localized Electronic Excitations in Phenylacetylene Dendrimers. *J. Phys. Chem. B* **1998**, *102*, 3310−3315.
(64) Kilina, S.; Tretiak, S.; Doorn, S. K.; Luo, Z.; Papadimitrakopoulos, F.; Piryatinski, A.; Saxena, A.; Bishop, A. R. Cross-Polarized Excitons in Carbon Nanotubes. *Proc. Natl. Acad. Sci. U. S. A.* **2008**, *105*, 6797−6802.
(65) Kilina, S.; Tretiak, S. Excitonic and Vibrational Properties of Single-Walled Semiconducting Carbon Nanotubes. *Adv. Funct. Mater.* **2007**, *17*, 3405−3420.
(66) Tully, J. C. Molecular Dynamics with Electronic Transitions. *J. Chem. Phys.* **1990**, *93*, 1061−1071.
(67) Nelson, T.; Fernandez-Alberti, S.; Roitberg, A. E.; Tretiak, S. Nonadiabatic Excited-State Molecular Dynamics: Treatment of Electronic Decoherence. *J. Chem. Phys.* **2013**, *138*, 224111.
(68) Subotnik, J. E.; Jain, A.; Landry, B.; Petit, A.; Ouyang, W.; Bellonzi, N. Understanding the Surface Hopping View of Electronic Transitions and Decoherence. *Annu. Rev. Phys. Chem.* **2016**, *67*, 387−417.
(69) Fernandez-Alberti, S.; Roitberg, A. E.; Nelson, T.; Tretiak, S. Identification of Unavoided Crossings in Nonadiabatic Photoexcited

DOI: 10.1021/acs.jctc.8b00103
J. Chem. Theory Comput. 2018, 14, 3955−3966

Dynamics Involving Multiple Electronic States in Polyatomic Conjugated Molecules. *J. Chem. Phys.* **2012**, *137*, 014512.
(70) Bjorgaard, J. A.; Velizhanin, K. A.; Tretiak, S. Nonequilibrium Solvent Effects in Born-Oppenheimer Molecular Dynamics for Ground and Excited Electronic States. *J. Chem. Phys.* **2016**, *144*, 154104.
(71) Nelson, T.; Naumov, A.; Fernandez-Alberti, S.; Tretiak, S. Nonadiabatic Excited-State Molecular Dynamics: On-The-Fly Limiting of Essential Excited States. *Chem. Phys.* **2016**, *481*, 84.
(72) Klamt, A.; Schüürmann, G. COSMO: A New Approach to Dielectric Screening in Solvents with Explicit Expressions for the Screening Energy and its Gradient. *J. Chem. Soc., Perkin Trans. 2* **1993**, 799−805.
(73) Barone, V.; Cossi, M. Quantum Calculation of Molecular Energies and Energy Gradients in Solution by a Conductor Solvent Model. *J. Phys. Chem. A* **1998**, *102*, 1995−2001.
(74) Rauscher, U.; Bässler, H.; Bradley, D.; Hennecke, M. Exciton Versus Band Description of the Absorption and Luminescence Spectra in Poly(p-phenylenevinylene). *Phys. Rev. B: Condens. Matter Mater. Phys.* **1990**, *42*, 9830.
(75) Burroughes, J.; Bradley, D.; Brown, A.; Marks, R.; Mackay, K.; Friend, R.; Burns, P.; Holmes, A. Light-Emitting Diodes Based on Conjugated Polymers. *Nature* **1990**, *347*, 539−541.
(76) Vestweber, H.; Greiner, A.; Lemmer, U.; Mahrt, R. F.; Richert, R.; Heitz, W.; Bässler, H. Progress Towards Processible Materials for Light-Emitting Devices using Poly(p-phenylphenylenevinylene). *Adv. Mater.* **1992**, *4*, 661−662.
(77) Cornil, J.; Beljonne, D.; Shuia, Z.; Hagler, T.; Campbell, I.; Bradley, D.; Brédas, J.; Spangler, C.; Müllen, K. Vibronic Structure in the Optical Absorption Spectra of Phenylene Vinylene Oligomers: A Joint Experimental and Theoretical Study. *Chem. Phys. Lett.* **1995**, *247*, 425−432.
(78) Bazan, G. C.; Oldham, W. J.; Lachicotte, R. J.; Tretiak, S.; Chernyak, V.; Mukamel, S. Stilbenoid Dimers: Dissection of a Paracyclophane Chromophore. *J. Am. Chem. Soc.* **1998**, *120*, 9188−9204.
(79) Frolov, S.; Bao, Z.; Wohlgenannt, M.; Vardeny, Z. V. Ultrafast Spectroscopy of Even-Parity States in π-Conjugated Polymers. *Phys. Rev. Lett.* **2000**, *85*, 2196.
(80) Peeters, E.; Ramos, A. M.; Meskers, S. C.; Janssen, R. A. Singlet and Triplet Excitations of Chiral Dialkoxy-p-phenylene Vinylene Oligomers. *J. Chem. Phys.* **2000**, *112*, 9445−9454.
(81) Lira-Cantu, M.; Krebs, F. C. Hybrid Solar Cells Based on MEH-PPV and Thin Film Semiconductor Oxides (TiO_2, Nb_2O_5, ZnO, CeO_2 and CeO_2-TiO_2): Performance Improvement During Long-Time Irradiation. *Sol. Energy Mater. Sol. Cells* **2006**, *90*, 2076−2086.
(82) Nielsen, C. B.; Angerhofer, A.; Abboud, K. A.; Reynolds, J. R. Discrete Photopatternable π-Conjugated Oligomers for Electrochromic Devices. *J. Am. Chem. Soc.* **2008**, *130*, 9734−9746.
(83) Ellinger, S.; et al. Donor-Acceptor-Donor-Based π-Conjugated Oligomers for Nonlinear Optics and Near-IR Emission. *Chem. Mater.* **2011**, *23*, 3805−3817.
(84) Panda, A. N.; Plasser, F.; Aquino, A. J.; Burghardt, I.; Lischka, H. Electronically Excited States in Poly(p-phenylenevinylene): Vertical Excitations and Torsional Potentials from High-Level Ab Initio Calculations. *J. Phys. Chem. A* **2013**, *117*, 2181−2189.
(85) Park, Y. I.; Kuo, C.-Y.; Martinez, J. S.; Park, Y.-S.; Postupna, O.; Zhugayevych, A.; Kim, S.; Park, J.; Tretiak, S.; Wang, H.-L. Tailored Electronic Structure and Optical Properties of Conjugated Systems through Aggregates and Dipole-Dipole Interactions. *ACS Appl. Mater. Interfaces* **2013**, *5*, 4685−4695.
(86) Park, Y.; et al. A New pH Sensitive Fluorescent and White Light Emissive Material Through Controlled Intermolecular Charge Transfer. *Chem. Sci.* **2015**, *6*, 789−797.
(87) Badaeva, E. A.; Timofeeva, T. V.; Masunov, A.; Tretiak, S. Role of Donor-Acceptor Strengths and Separation on the Two-Photon Absorption Response of Cytotoxic Dyes: A TD-DFT Study. *J. Phys. Chem. A* **2005**, *109*, 7276−7284.
(88) Frisch, M. J.; et al. *Gaussian 09*, revision D.02; Gaussian, Inc.: 2009.
(89) Humphrey, W.; Dalke, A.; Schulten, K. VMD: Visual Molecular Dynamics. *J. Mol. Graphics* **1996**, *14*, 33−38.
(90) Wu, C.; Malinin, S. V.; Tretiak, S.; Chernyak, V. Y. Exciton Scattering and Localization in Branched Dendrimeric Structures. *Nat. Phys.* **2006**, *2*, 631−635.
(91) Li, Y.; Ullrich, C. Time-Dependent Transition Density Matrix. *Chem. Phys.* **2011**, *391*, 157−163.
(92) Nelson, T.; Fernandez-Alberti, S.; Roitberg, A. E.; Tretiak, S. Conformational Disorder in Energy Transfer: Beyond Förster Theory. *Phys. Chem. Chem. Phys.* **2013**, *15*, 9245−9256.
(93) Baer, M. *Beyond Born-Oppenheimer: Electronic Nonadiabatic Coupling Terms and Conical Intersections*; John Wiley & Sons: 2006.
(94) Cardozo, T. M.; Aquino, A. J.; Barbatti, M.; Borges, I., Jr; Lischka, H. Absorption and Fluorescence Spectra of Poly(p-phenylenevinylene) (PPV) Oligomers: An Ab Initio Simulation. *J. Phys. Chem. A* **2015**, *119*, 1787−1795.
(95) Matsika, S.; Krause, P. Nonadiabatic Events and Conical Intersections. *Annu. Rev. Phys. Chem.* **2011**, *62*, 621−643.
(96) Marder, S. R.; Gorman, C. B.; Meyers, F.; Perry, J. W.; Bourhill, G.; Brédas, J.-L.; Pierce, B. M. A Unified Description of Linear and Nonlinear Polarization in Organic Polymethine Dyes. *Science* **1994**, *265*, 632−635.

DOI: 10.1021/acs.jctc.8b00103
J. Chem. Theory Comput. 2018, 14, 3955−3966